

1 **Improving hydrological projection performance under contrasting**  
2 **climatic conditions using spatial coherence through a hierarchical**  
3 **Bayesian regression framework**

4 **Zhengke Pan<sup>a,b</sup>, Pan Liu<sup>a,b,\*</sup>, Shida Gao<sup>a,b</sup>, Jun Xia<sup>a,b,c</sup>, Jie Chen<sup>a,b</sup>, Lei Cheng<sup>a,b</sup>**

5

6 <sup>a</sup>State Key Laboratory of Water Resources and Hydropower Engineering Science, Wuhan  
7 University, Wuhan 430072, China

8

9 <sup>b</sup>Hubei Provincial Collaborative Innovation Center for Water Resources Security, Wuhan 430072,  
10 China

11 <sup>c</sup>Chinese Academy of Sciences, Beijing 100864, China

12

13 \*Corresponding author. Email: [liupan@whu.edu.cn](mailto:liupan@whu.edu.cn); Tel: +86-27-68775788; Fax:  
14 +86-27-68773568

15

16

17

18

19

20 **ABSTRACT**

21 Understanding the projection performance of hydrological models under contrasting  
22 climatic conditions supports robust decision making, which highlights the need to  
23 adopt time-varying parameters in hydrological modeling to reduce performance  
24 degradation. Many existing literatures model the time-varying parameters as functions  
25 of physically-based covariates; however, a major challenge remains in finding  
26 effective information to control the large uncertainties that are linked to the additional  
27 parameters within the functions. This paper formulated the time-varying parameters  
28 for a lumped hydrological model as explicit functions of temporal covariates and used  
29 a hierarchical Bayesian (HB) framework to incorporate the spatial coherence of  
30 adjacent catchments to improve the robustness of the projection performance. Four  
31 modeling scenarios with different spatial coherence schemes, and one scenario with a  
32 stationary scheme for model parameters, were used to explore the transferability of  
33 hydrological models under contrasting climatic conditions. Three spatially adjacent  
34 catchments in southeast Australia were selected as case studies to examine the validity  
35 of the proposed method. Results showed that (1) the time-varying function improved  
36 the model performance but also amplified the projection uncertainty compared with  
37 stationary setting of model parameters; (2) the proposed HB method successfully  
38 reduced the projection uncertainty and improved the robustness of model performance;  
39 and (3) model parameters calibrated over dry years were not suitable for predicting  
40 runoff over wet years because of a large degradation in projection performance. This  
41 study improves our understanding of the spatial coherence of time-varying parameters,  
42 which will help improve the projection performance under differing climatic  
43 conditions.

44 **Keywords:** Climate change; Hierarchical Bayesian; Hydrological model parameters;  
45 Spatial coherence; Streamflow projection; Contrasting climatic conditions

46

47

## 48 **1. INTRODUCTION**

49 Long-term streamflow projection is an important part of effective water  
50 resources planning because it can predict future scarcity in water supply and help  
51 prevent floods. Streamflow projections typically involve the following: (i) calibrating  
52 hydrological model parameters with partial historical observations (e.g., precipitation,  
53 evaporation, and streamflow); (ii) projecting streamflow under periods that are  
54 outside of those for model calibration; and (iii) evaluating the model projection  
55 performance with certain criteria. One of the most basic assumptions of this  
56 process—that the calibrated model parameters are stationary and can be applied to  
57 predict catchment behaviors in the near future, has been widely questioned (Brigode  
58 et al., 2013; Broderick et al., 2016; Chiew et al., 2014; Chiew et al., 2009; Ciais et al.,  
59 2005; Clarke, 2007; Cook et al., 2004; Coron et al., 2012; Deng et al., 2016; Merz et  
60 al., 2011; Moore and Wondzell, 2005; Moradkhani et al., 2012; Moradkhani et al.,  
61 2005; Pathiraja et al., 2016; Pathiraja et al., 2018; Patil and Stieglitz, 2015; Westra et  
62 al., 2014; Xiong et al., 2019; Zhang et al., 2018).

63 Many previous studies have explored the transferability of stationary parameters  
64 to periods with different climatic conditions. They have concluded that hydrological  
65 model parameters are sensitive to the climatic conditions of the calibration period  
66 (Chiew et al., 2014; Chiew et al., 2009; Coron et al., 2012; Merz et al., 2011; Renard  
67 et al., 2011; Seiller et al., 2012; Vaze et al., 2010). For instance, Merz et al. (2011)  
68 calibrated model parameters using six consecutive 5-year periods between 1976 and  
69 2006 for 273 catchments in Austria and found that the calibrated parameters

70 representing snow and soil moisture processes showed a significant trend in the study  
71 area. Other studies have found that degradation in model performance was directly  
72 related to the difference in precipitation between the calibration and verification  
73 periods(Coron et al., 2012; Vaze et al., 2010). One proposal for managing this  
74 problem is to calibrate model parameters in periods with similar climatic conditions to  
75 the near future, but future streamflow observations are unavailable. Thus, it is still  
76 necessary to reduce the magnitude of performance loss and improve the robustness of  
77 the projection performance using calibrated parameters based on the historical records,  
78 even though the climatic conditions in the future may be dissimilar to those used for  
79 model calibration.

80 Several recent studies have found that hydrological models with time-varying  
81 parameters exhibited a significant improvement in its projection performance  
82 compared with the stationary parameters(Deng et al., 2016; Deng et al., 2018; Westra  
83 et al., 2014). The functional method is one of the most promising ways to model  
84 time-varying parameters and shows its excellence in improving the model projection  
85 performance(Guo et al., 2017; Westra et al., 2014; Wright et al., 2015). This method  
86 models the time-varying parameter(s) as the function(s) of physically-based  
87 covariates (e.g., temporal covariate and Normalized Difference Vegetation Index).  
88 Generally, the hydrological model is run with various assumed functions, the best  
89 functional forms of time-varying parameters can be obtained by comparing the  
90 evaluation criteria. However, a major challenge for the application of the functional  
91 method remains in finding effective information to control the large uncertainties that

92 are linked to the additional parameters describing these regression functions.

93 Similarity of adjacent catchments has been verified its validity in controlling the  
94 estimation uncertainty of model parameters (Bracken et al., 2018; Cha et al., 2016;  
95 Cooley et al., 2007; Lima and Lall, 2009; Najafi and Moradkhani, 2014; Sun and Lall,  
96 2015; Sun et al., 2015; Yan and Moradkhani, 2015). The level of similarity of  
97 different catchments is known as spatial coherence. For instance, Sun and Lall (2015)  
98 used the spatial coherence of trends in annual maximum precipitation in the United  
99 States, and successfully reduced the parameter estimation uncertainty in their at-site  
100 frequency analysis. In general, there are three methods to consider the spatial  
101 coherence between different catchments in parameter estimation. The first one is no  
102 pooling, which means every catchment is modeled independently, and all parameters  
103 are catchment-specific. The second one is complete pooling, which means all  
104 parameters are considered to be common across all catchments. The third/last one is  
105 hierarchical Bayesian (HB) framework, also known as partial pooling, which means  
106 some parameters are allowed to vary by catchments and some parameters are assumed  
107 to drown from a common hyper-distribution across the region that consists of  
108 different catchments. In these three approaches, the HB framework has been proved  
109 as the most efficient method to incorporate the spatial coherence to reduce the  
110 estimation uncertainty because it has the advantage of shrinking the local parameter  
111 toward the common regional mean and including an estimation of its variance or  
112 covariance across the catchments (Bracken et al., 2018; Sun and Lall, 2015; Sun et al.,  
113 2015). In the field of hydrological modeling, most proceeding literatures were focused

114 on no pooling models that neglect the spatial coherence between catchments  
115 (Heuvelmans et al., 2006; Lebecherel et al., 2016; Merz and Blöschl, 2004; Oudin et  
116 al., 2008; Singh et al., 2012; Tegegne and Kim, 2018; Xu et al., 2018); little attention  
117 has been paid to the HB framework. Thus, we want to fill this gap and explore the  
118 applicability of the spatial coherence through the HB framework in hydrological  
119 modeling with the time-varying parameters.

120 The objectives of this paper were to: (1) verify the effect of the time-varying  
121 model parameter scheme on model projection performance and uncertainty analysis  
122 compared with stationary model parameters; (2) verify the projection performance of  
123 considering spatial coherence of adjacent catchments through the HB framework  
124 compared with spatial incoherence; and (3) compare the model projection  
125 performance for different climatic transfer schemes.

126 The rest of the paper is organized as follows. Section 2 outlines the methodology  
127 employed in this study including differential split sample test (DSST) for segmenting  
128 the historical series, the hydrological model, and the two-level HB framework for  
129 incorporating spatial coherence from adjacent catchments. Section 3 presents the  
130 information on the study area and data. The results and discussion are described in  
131 section 4. Section 5 summarizes the main conclusions of the study.

## 132 **2. METHODOLOGY**

133 The methodology is outlined by a flowchart in Figure 1, and is summarized as  
134 follows:

135 (1) A temporal parameter transfer scheme is implemented (described in section

136 2.1) using a classic DSST procedure in which the available data are divided into wet  
137 and dry years;

138 (2) A daily conceptual rainfall-runoff model is used (outlined in section 2.2);

139 (3) A two-level HB framework is used to incorporate spatial coherence in  
140 hydrological modeling (described in section 2.3). The process layer (first level) of the  
141 framework models the temporal variation in the model parameters using a  
142 time-varying function, while the prior layer (second level) models the spatial  
143 coherence of the regression parameters in the time-varying function. Four modeling  
144 scenarios with different spatial coherence schemes, and one scenario with a stationary  
145 scheme for the model parameters, are used to evaluate the transferability of  
146 hydrological models under contrasting climatic conditions;

147 (4) Likelihood function and parameter estimation methods are applied (outlined  
148 in section 2.4); and

149 (5) The criteria are used to evaluate the model performance for various model  
150 scenarios (described in section 2.5).

## 151 **2.1 Differential split sampling test**

152 To verify the projection performance of the rainfall-runoff model under  
153 contrasting climatic conditions (wet and dry years), a classic DSST using annual  
154 rainfall records was adopted.

155 Two separate tasks were needed to develop the DSST method into a working  
156 system. The first step was to define “dry years”. The method to define the dry years is  
157 adopted from Saft et al. (2015), which is a rigorous identification method that treats

158 autocorrelation in the regression residuals, undertakes global significance testing, and  
159 defines the start and end of the droughts individually for each catchment. Saft et al.  
160 (2015) tested several algorithms for dry years delineation, which considered different  
161 combinations of dry run length, dry run anomaly and various boundary criteria, and  
162 found that the identification results of dry years by one of the algorithms showed  
163 marginal dependence on the algorithm and the main results were robust to different  
164 algorithms. The detailed processes could be found on Saft et al. (2015) and also are  
165 generalized as follows.

166 Firstly, the annual rainfall data were calculated relative to the annual mean, and  
167 the anomaly series was divided by the mean annual rainfall and smoothed with a  
168 3-year moving window. Secondly, the first year of the drought remained the start of  
169 the first 3 years negative anomaly period. Thirdly, the exact end date of the dry years  
170 was determined through analysis of the unsmoothed anomaly data from the last  
171 negative 3-year anomaly. The end year was identified as the last year of this 3 year  
172 period unless: (i) there was a year with a positive anomaly  $>15\%$  of the mean, in  
173 which case the end year is set to the year prior to that year; or (ii) if the last two years  
174 have slightly positive anomalies (but each  $<15\%$  of the mean), in which case the end  
175 year is set to the first year of positive anomaly; (iii) to ensure that the dry years are  
176 sufficiently long and severe, in the subsequent analysis, the authors use dry years with  
177 the following characteristics: length  $\geq 7$  years; mean dry years anomaly  $<-5\%$ .

178 In the second step, the wet years were defined as the complement of the dry  
179 years in the historical records. A similar approach to define the dry and wet years was



180 used by Fowler et al. (2016).

181 In the DSST method, the model parameters calibrated in the wet years were  
182 evaluated in the dry years, and vice versa. In addition, criteria, i.e,  $NSE_{\text{sqrt}}$ , BIAS, DIC,  
183 [MaxF](#), and [MinF](#) illustrated in section 2.5, were used to evaluate the performance of  
184 the calibrated parameters for different transfer schemes.

## 185 **2.2 The rainfall-runoff model**

186 The hydrological model used in this study is the GR4J (modèle du Génie Rural à  
187 4 paramètres Journalier), which is a lumped conceptual rainfall-runoff model (Perrin  
188 et al., 2003). The original version of the GR4J model (Figure 2) comprised four  
189 parameters (Perrin et al., 2003): production store capacity ( $\theta_1$  mm), groundwater  
190 exchange coefficient ( $\theta_2$  mm), 1-day-ahead maximum capacity of the routing store  
191 ( $\theta_3$  mm), and the time base of the unit hydrograph ( $\theta_4$  days). More details on the  
192 GR4J model can be found in Perrin et al. (2003).

193 The GR4J model is a parsimonious, but efficient model. The model has been  
194 used successfully across a wide range of hydro-climatic conditions across the world,  
195 including the crash testing of model performance under contrasting climatic  
196 conditions (Coron et al., 2012), and the simulation of runoff for revisiting the  
197 deficiency in insufficient model calibration (Fowler et al., 2016). For example, Fowler  
198 et al. (2016) verified that conceptual rainfall-runoff models were more capable under  
199 changing climatic conditions than previously thought. These characteristics make the  
200 GR4J particularly suitable as a starting point for implementing modifications and/or  
201 improving predictive ability under changing climatic conditions.

## 202 **2.3 The HB framework for the time-varying model parameter**

203 In this study, various versions were constructed for evaluating the projection  
204 capabilities of models for contrasting climatic conditions (wet and dry years), and for  
205 considering the temporal variation and spatial coherence of parameter  $\theta_1$ .

### 206 2.3.1 Process layer: temporal variation of the model parameter

207 As described in the literature (Pan et al., 2019; Perrin et al., 2003; Renard et  
208 al., 2011; Westra et al., 2014), parameter  $\theta_1$ , which represents the primary storage  
209 of water in the catchment, is the most sensitive parameter in the GR4J model  
210 structure, and the stochastic variations of this parameter have the largest impact on  
211 model projection performance (Renard et al., 2011; Westra et al., 2014). In addition,  
212 the temporal variation in the catchment storage capacity was physically  
213 interpretable. Periodic variations in the production store capacity  $\theta_1$  can be  
214 induced by the periodicity in precipitation and in seasonal vegetation growth and  
215 senescence. In the present study,  $\theta_1$  was constructed to account for the periodical  
216 variation that had a significant impact on the extensionality of the model. The  
217 periodical variation in catchment storage capacity  $\theta_1$  is described by a sine function,  
218 using amplitude and frequency.

219 Thus, for any catchment  $c$ , the full temporal regression function for  $\theta_1$  at the  
220 process layer is:

$$221 \text{ Process layer: } \theta_1(c, t) = \alpha(c) + \beta(c) \sin[\omega(c)t] \quad (1)$$

222 where  $\alpha$ ,  $\beta$ ,  $\omega$  are regression parameters for the specific DSST method, and  $\alpha$   
223 signifies the intercept, and  $\{\beta, \omega\}$  represents the amplitude and frequency of the

224 sine function, respectively.  $t$  is the time step. According to the definition of the GR4J  
 225 model (Perrin et al., 2003), the value of  $\theta_1$  must be a positive value. If model  
 226 parameter  $\theta_1$  is constant then  $\beta=0$ ,  $\alpha>0$  suffice in Eq.1. Meanwhile, the value  
 227 of  $\omega$  becomes irrelevant. Thus, the resulting model simplifies to a stationary  
 228 hydrological model.

### 229 2.3.2 Prior layer: spatial coherence of regression parameters

230 For a heterogeneous region that is distinctly non-uniform in climatic and  
 231 geologic conditions, different catchments within the region typically have different  
 232 catchment storage capacities and different values of production store capacity  $\theta_1$ .  
 233 For a homogeneous region prescribed by similar climatic and geologic conditions in  
 234 each part, the production store capacity (in Eq. 1) is expected to be the same among  
 235 different catchments of the region. The model could be improved by considering  
 236 spatial input, i.e., the spatial coherence of parameters across adjacent catchments  
 237 (Chen et al., 2014; Lima et al., 2016; Merz and Blöschl, 2004; Oudin et al., 2008;  
 238 Patil and Stieglitz, 2015; Renard et al., 2011; Sun et al., 2014).

239 In this study, independent Gaussian prior distributions were used for the  
 240 amplitude  $\beta$  and frequency  $\omega$  at the prior layer to include the potential spatial  
 241 coherence. Their equations are as follows:

$$\begin{aligned}
 \text{242} \quad \text{Prior layer:} \quad \beta(c) &= N(\mu_2, \sigma_2^2) \\
 \omega(c) &= N(\mu_3, \sigma_3^2)
 \end{aligned}
 \tag{2}$$

243 where  $\mu_2$ ,  $\mu_3$ ,  $\sigma_2$  and  $\sigma_3$  are hyper-parameters, and  $N(\cdot)$  represents the  
 244 hyper-distribution, i.e., a Gaussian distribution. Independent Gaussian distributions

245 were assumed for the amplitude  $\beta$  and frequency  $\omega$  that were used to model  
246 spatial coherence based on practical considerations. The prior layer of the HB  
247 framework aims to describe the variation of  $\{\beta, \omega\}$  in space by means of a Gaussian  
248 spatial process in which the mean value depends on covariates describing regional  
249 characteristics. Amplitude  $\beta$  and frequency  $\omega$  are the most important parameters  
250 in the regression function and can reflect the spatial connection of variation and  
251 cyclicity of catchment production storage capacity among catchments. The Gaussian  
252 distribution is one of the widely used distributions for describing the prior layer  
253 within the HB framework and has been applied in many previous studies, such as Sun  
254 et al (2015, 2016) and Chen et al (2014). In addition, the introduction of the Gaussian  
255 distributions to describe the spatial coherence of  $\beta$  and  $\omega$  also because that there  
256 are still uncountable factors that may have impacts on the spatial coherence between  
257 adjacent catchments, which might make the coherence tend to converge a central  
258 value but with finite variance, and obey the Central limit theorem.

### 259 2.3.3 Modeling scenarios

260 Five modeling scenarios (Table 1) were carried out to assess the effect of spatial  
261 coherence on the time-varying function. Different levels of spatial coherence of  
262  $\{\beta, \omega\}$  were assumed in scenarios 1 to 4, while in scenario 5 parameter  $\theta_1$  was set  
263 to be constant to provide a comparison. It should be noted that the estimates for  
264 spatially coherent regression parameters would be shared by different catchments  
265 while other quantities would be regarded as catchment-specific variables. For  
266 example, amplitude  $\beta$  is spatially linked in scenario 1, i.e.,  $\beta(c) = N(\mu_2, \sigma_2^2)$ , which

267 means that the estimates of  $\beta$  are shared by all catchments. Meanwhile, regression  
 268 parameters  $\omega_{1-1}$ ,  $\omega_{1-2}$ , and  $\omega_{1-3}$  are used as independent variables to represent the  
 269 frequency of model parameter  $\theta_1$  in different catchments. The number of unknown  
 270 quantities in different scenarios are as follows: fifteen in scenarios 1 and 2, thirteen in  
 271 scenario 3 and eighteen in scenario 4. The prior ranges of all unknown quantities  
 272 (including model parameters ( $\theta_2$ ,  $\theta_3$ , and  $\theta_4$ ), regression parameters  $\alpha$ ,  $\beta$  and  
 273  $\omega$ , and hyper-parameters  $\mu_2$ ,  $\sigma_2$ ,  $\mu_3$  and  $\sigma_3$ ) in different scenarios and both  
 274 DSST schemes could be found in Table S1 in Supplement material. It should be noted  
 275 that in a specific scenario, some unknown quantities might not exist. For example,  $\mu_3$   
 276 and  $\sigma_3$  did not exist in scenario 1 while  $\mu_2$  and  $\sigma_2$  did not exist in scenario  
 277 2.

## 278 2.4 Estimation and projection

279 The objective function and parameter inference methods were used to derive the  
 280 posterior distribution of all unknown quantities, as illustrated below.

### 281 2.4.1 Objective function

282 For a specific catchment, the model parameters were calibrated to minimize the  
 283 following objective function, which was adopted from Coron et al. (2012).

$$284 \quad \varepsilon_c [\theta_1, \theta_2, \theta_3, \theta_4] = -RMSE[\sqrt{Q}] (1 + |1 + BIAS|) \quad (3)$$

285 where

$$286 \quad RMSE[\sqrt{Q}] = \sqrt{\frac{1}{T} \sum_{t=1}^T [Q_{sim}(t) - Q_{obs}(t)]^2} \quad (4)$$

287 and  $RMSE[\sqrt{Q}]$  refers to the root-mean-square error, in which  $Q_{sim}$  is derived by  
 288 the adopted hydrological model.  $T$  represents the number of the time series while  $t$  is

289 the time step.

290 Coron et al. (2012) showed that this objective function performed well. In this  
291 function, the combination of  $RMSE[\sqrt{Q}]$  and  $BIAS$  (Eq.7) gives weight to dynamic  
292 representation as well as the water balance. Using square-root-transformed flows to  
293 compute the RMSE reduces the influence of high flows during the calibration period  
294 and provides a good compromise between alternative criteria.

295 In the case of multiple catchments, the objective function of the HB framework  
296 was the product of Eq.3 and the conditional probability of spatial coherence of  
297 regression parameters  $f_N$ . It was written as follows:

$$\text{Scenario 1: } \Lambda = \prod_{c=1}^C \varepsilon_c \left[ \theta_1(t,c), \theta_2(c), \theta_3(c), \theta_4(c) \mid \alpha(c), \beta, \omega(c) \right] \bullet f_N(\beta \mid \mu_2, \sigma_2)$$

$$\text{Scenario 2: } \Lambda = \prod_{c=1}^C \varepsilon_c \left[ \theta_1(t,c), \theta_2(c), \theta_3(c), \theta_4(c) \mid \alpha(c), \beta(c), \omega \right] \bullet f_N(\omega \mid \mu_3, \sigma_3)$$

298  $\text{Scenario 3: } \Lambda = \prod_{c=1}^C \varepsilon_c \left[ \theta_1(t,c), \theta_2(c), \theta_3(c), \theta_4(c) \mid \alpha(c), \beta, \omega \right] \bullet \prod_{n=1}^2 f_N(\beta, \omega \mid \mu_2, \sigma_2, \mu_3, \sigma_3) \quad (5)$

$$\text{Scenario 4: } \Lambda = \prod_{c=1}^C \varepsilon_c \left[ \theta_1(t,c), \theta_2(c), \theta_3(c), \theta_4(c) \right]$$

$$\text{Scenario 5: } \Lambda = \prod_{c=1}^C \varepsilon_c \left[ \theta_1(c), \theta_2(c), \theta_3(c), \theta_4(c) \right]$$

299 where the number of catchments in the region is represented by  $C$ , and the Gaussian  
300 spatial function between regression parameters  $\beta, \omega$  and hyper-parameters  $\mu_2$ ,  
301  $\mu_3$ ,  $\sigma_2$  and  $\sigma_3$  are denoted by  $f_N()$ .  $N$  refers to the Gaussian distribution and  
302  $n$  represents the number of regression parameters that are spatially coherent.

### 303 2.4.2 Inference

304 The uniform distribution is used as the prior distribution for hyper-parameters  
305 and spatially irrelevant parameters. Meanwhile, spatially relevant parameters are  
306 sampled from the Gaussian distributions. Because the prior distribution has no impact

307 on the final evaluation of different scenarios, the prior distributions are not presented  
308 in Eq.5. The likelihood functions defined in Eqs. 3 and 5 pose a computational  
309 challenge because their dimensionality grows (primarily related to the number of  
310 catchment-specific parameters) with the number of catchments considered. The  
311 unknown quantities, including model parameters ( $\theta_2, \theta_3$ , and  $\theta_4$ ), regression  
312 parameters  $\alpha$ ,  $\beta$  and  $\omega$ , and hyper-parameters  $\mu_2$ ,  $\sigma_2$ ,  $\mu_3$  and  $\sigma_3$  (if  
313 presents), are sampled and estimated simultaneously using the Shuffled Complex  
314 Evolution Metropolis (SCEM-UA) sampling method (Ajami et al., 2007; Vrugt et al.,  
315 2003; Vrugt et al., 2009). The SCEM-UA sampling method is a widely used Markov  
316 Chain Monte Carlo algorithm for simulating the posterior probability distribution of  
317 parameters that are conditional on the current choice of parameters and data. When  
318 compared with traditional Metropolis-Hasting samplers, the SCEM-UA algorithm  
319 more efficiently reduces the number of model simulations needed to infer the  
320 posterior distribution of parameters, (Ajami et al., 2007; Duan et al., 2007; Liu et al.,  
321 2014; Liu and Gupta, 2007; Vrugt et al., 2003). Convergence is assessed by evolving  
322 three parallel chains with 30000 random samples, the posterior distributions of  
323 parameters are evaluated by the Gelman-Rubin convergence value and are confirmed  
324 that the convergence value is smaller than the threshold 1.2 (Gelman et al., 2013).

## 325 **2.5 Model performance criteria**

326 Five criteria were used to assess the projection performance during the  
327 verification periods.

328 (1) The first criterion was  $NSE_{\text{sqrt}}$ , known as the arithmetic square root of

329 Nash-Sutcliffe Efficiency (Coron et al., 2012; Moriasi et al., 2007; Nash and Sutcliffe,  
 330 1970). When compared with the classic NSE,  $NSE_{sqr}$  gives an intermediate, more  
 331 balanced picture of the overall hydrograph fit because it can reduce the influence of  
 332 high flow. It is expressed as:

$$333 \quad NSE_{sqr} = 1 - \frac{\sum_{t=1}^T \left[ \sqrt{Q_{obs}(t)} - \sqrt{Q_{sim}(t)} \right]^2}{\sum_{t=1}^T \left[ \sqrt{Q_{obs}(t)} - \sqrt{\bar{Q}_{obs}} \right]^2} \quad (6)$$

334 where  $Q_{sim}(t)$  and  $Q_{obs}(t)$  represent the simulated and observed daily streamflow  
 335 values for the  $t^{\text{th}}$  day, respectively;  $\bar{Q}_{obs}$  is the mean of the observed daily streamflow  
 336 for the calculation interval, and  $T$  refers to the length of the calculation period.

337 (2) The second criterion is the BIAS, [one of the most popular indexes to reflect](#)  
 338 [the deviation degree between the modeled runoff and observations](#), also is a part of  
 339 the objective function Eq.3.

$$340 \quad BIAS = \frac{\sum_{t=1}^T [Q_{sim}(t) - Q_{obs}(t)]}{\sum_{t=1}^T [Q_{obs}(t)]} \quad (7)$$

341 (3) The third criterion is the Deviance information criterion (DIC), which was  
 342 defined by Spiegelhalter et al. (2002). It is a widely used and popular measure  
 343 designed for Bayesian model comparison and is a Bayesian alternative to the standard  
 344 Akaike Information Criterion. The DIC value for a Bayesian scenario is obtained as:

$$345 \quad DIC = -2 \log \left( p \left( q \mid \theta_{Bayes}, \xi \right) \right) + 2 p_{DIC} \quad (8)$$

346 where  $p_{DIC}$  is the effective number of parameters, defined as

$$347 \quad p_{DIC} = 2 \left( \log \left( p \left( q \mid \theta_{Bayes}, \xi \right) \right) - \frac{1}{S} \sum_{s=1}^S \log \left( p \left( q \mid \theta^s, \xi \right) \right) \right) \quad (9)$$



348 where  $p$  refers to probability,  $q$  represents the observations of streamflow and  $\xi$   
349 denotes the time series of model input, e.g., rainfall and potential evapotranspiration.  
350 Posterior mean  $\theta_{Bayes} = \text{Expect}(\theta|q, \xi)$  and  $s=1, \dots, S$ , means the sequence number of  
351 the simulated parameter set  $\theta^s$  by the adopted SCEM-UA algorithm. According to  
352 Spiegelhalter et al. (2002), scenarios with smaller DIC would be preferred to  
353 scenarios with larger DIC.

354 (4) The fourth and fifth criteria are the Mean annual maximum flow (MaxF,  
355 mm/d) and Mean annual minimum flow (MinF, mm/d), which are used to qualify the  
356 performance of the high flows and low flows. These criteria are self-explanatory and  
357 have been used in many studies to assess the magnitude of maximum and minimum  
358 levels of flows (Ekstrom et al., 2018). The scenarios with the least absolute variation  
359 between the modeled values and the observed values are recognized as the best  
360 scenarios.

### 361 **3. Study area and data**

362 To evaluate the model performance, we used daily precipitation (mm/day),  
363 potential evapotranspiration (mm/day), and streamflow (mm/day) time series records  
364 for three unregulated and unimpaired catchments in south-eastern Australia, taken  
365 from the national dataset of Australia (Zhang et al., 2013), covering 1976–2011. The  
366 streams were unregulated: they were not subject to dam or reservoir regulations,  
367 which can reduce the impact of human activity. The observed streamflow record  
368 contained at least 11835 daily observations (equivalent to record integrity of greater  
369 than 90%) for 1976–2011, with acceptable data quality. The first complete year of

370 data was used for model warm-up to reduce the impact of the initial soil moisture  
371 conditions during the calibration period.

372 The attributes of the south-eastern Australian catchments are shown in Table 2  
373 and Figure 3. The IDs of these catchments are 225219 (Glencairn station on the  
374 Macalister River: mean annual rainfall, potential evapotranspiration, and runoff are  
375 1064 mm, 1142 mm, and 350 mm, respectively), 405219 (Dohertys station on the  
376 Goulburn River: mean annual rainfall, potential evapotranspiration, and runoff are  
377 1169 mm, 1193 mm, and 422 mm, respectively), and 405264 (D/S of Frenchman Ck  
378 Jun station on the Big River: mean annual rainfall, potential evapotranspiration, and  
379 runoff are 1406 mm, 1157 mm, and 469 mm, respectively). As shown in Figure 3,  
380 these catchments are adjacent to each other. All catchments experienced a severe  
381 multiyear drought around the end of the millennium. Saft et al. (2015) identified that  
382 the rainfall-runoff relationship in these catchments was altered during the long-term  
383 drought.

#### 384 **4. Results and discussion**

385 Results from the DSST were used to assess the model projection performance for  
386 five scenarios under contrasting climatic conditions. First, a DSST was conducted in  
387 each catchment to divide original records into [wet and dry years](#). Then, the projection  
388 performance for the five scenarios and associated parameter uncertainties were  
389 evaluated using the criteria described above.

## 390 **4.1 Dry years identification**

391 As illustrated in Table 3 and Figure 4, the drought definition method identified  
392 that the three catchments had similar dry years characteristics, with the same drought  
393 start (1997) and end (2009) points. The length of **dry years** for the studied catchments  
394 is same, 12 years. The mean **dry years'** anomaly was less severe in the Macalister  
395 catchment (225219), with a 6.95% reduction in the mean dry years' anomaly while the  
396 other two catchments experienced reductions of 9.84% (405219) and 9.62% (405264).

397 In terms of changes in rainfall, on average catchments had an 11% reduction  
398 from the wet years to the dry years (Table 3). Meanwhile, these catchments  
399 experienced a 17.6% decrease in runoff during the dry years, which is more severe  
400 than the reduction in rainfall. The similar findings can be derived out from the  
401 comparison of runoff coefficients of different periods, that is, all catchments  
402 experienced a decrease in its runoff coefficients during the dry years.

## 403 **4.2 Model performance in five scenarios**

404 As shown in Figures 5(a), 6(a) and 7, the calibrated model parameters yielded  
405 good simulation performance over the calibrated periods for all criteria. For example,  
406 the mean  $NSE_{\text{sqrt}}$  score during the calibration period across these catchments remained  
407 close to about 0.7 or slightly higher, regardless of which scenario was chosen.  
408 However, when the same parameter sets were verified by simulating streamflow over  
409 drier or wetter years, the model performance was degraded, including both the  
410 robustness and accuracy of projection performance. Furthermore, the magnitude of  
411 performance loss increases along with the **variation in rainfall** between the calibration

412 and verification periods.

413 Figure 5 shows the  $NSE_{\text{sqrt}}$  performance for calibration in wet years and  
414 verification in the dry years for each scenario in all catchments. All scenarios  
415 performed well in all catchments with the mean  $NSE_{\text{sqrt}}$  reaching 0.81 during the wet  
416 calibration period, and then all scenarios experienced a slight decrease in performance  
417 ( $NSE_{\text{sqrt}} = 0.75$ ) during the dry verification period. Scenario 4 (time-varying  
418 parameters without spatial inputs) or scenario 5 (temporally stable parameters)  
419 generally performed better during the calibration period than the scenarios that  
420 considered different levels of spatial coherence for the regression parameters. During  
421 the verification period, the  $NSE_{\text{sqrt}}$  rank order changed (Figure 5b). Scenario 4 had a  
422 higher median  $NSE_{\text{sqrt}}$  performance than scenario 5 in catchments 225219 and 405264.  
423 Although the median estimate in scenario 4 was slightly inferior to the latter in  
424 catchment 405219, its distribution of the  $NSE_{\text{sqrt}}$  performance was much more  
425 positively biased from the median estimates than scenario 5. Furthermore, the former  
426 reaches higher  $NSE_{\text{sqrt}}$  performance than the latter when comparing the top  $NSE_{\text{sqrt}}$   
427 performance of these two scenarios. Thus, it indicates the validity of the time-varying  
428 scheme for improving model performance. However, the introduction of additional  
429 regression parameters ( $\alpha, \beta$  and  $\omega$ ) at the same time amplified the model projection  
430 uncertainty in two of three catchments (405219 and 405264) when comparing results  
431 from scenarios 4 and 5. Fortunately, the appropriate adoption of spatial coherence  
432 alleviates this problem. In the DSST scheme of calibrating in the wet years and  
433 verifying in the dry years, scenario 2 exhibited the smallest fluctuation range of

434 NSE<sub>sqrt</sub> estimate in catchments 405219 and 405264 and was the second-best scenario  
435 in catchment 225219. Conversely, scenario 3 exhibited the smallest fluctuation range  
436 of NSE<sub>sqrt</sub> estimate in catchment 225219, and was the second-best scenario in  
437 catchments 405219 and 405264. As for the median NSE<sub>sqrt</sub> estimate, scenario 2 is the  
438 best scenario (which showed the best performance in catchment 225219 and 405219,  
439 but it was the fourth in catchment 405264), followed by scenario 3 (which is the  
440 second-best scenario in catchments 405219 and 405264 and is the third in catchment  
441 225219). In addition, the highest median NSE<sub>sqrt</sub> performance in scenarios 4 and 5  
442 during the calibration period did not guarantee the same superior performance during  
443 the verification period. This illustrates the deficiency of time-varying and stationary  
444 schemes of model parameters when spatial inputs from adjacent catchments are not  
445 considered.

446 Similarly, Figure 6 illustrates the NSE<sub>sqrt</sub> performance for each scenario in all  
447 catchments for calibration in the dry years and verification in the wet years. All  
448 scenarios performed well for all catchments with the mean NSE<sub>sqrt</sub> reaching 0.75 in  
449 the dry calibration period and 0.79 in the wet verification period. As shown in Figure  
450 6, models experienced a slight improvement in NSE<sub>sqrt</sub> performance when transferred  
451 from the dry years to the wet years. However, the projection performance calibrated  
452 using a contrasting climatic condition was inferior to the simulation performance that  
453 was directly calibrated from the climatic condition, compared with Figures 5(a) and  
454 6(b), or Figure 6(a) and 5(b). For example, the NSE<sub>sqrt</sub> performance in Figure 6(b) is  
455 inferior to that in Figure 5(a). By comparing scenarios in the calibration period, it was

456 found that scenarios 4 and 5 exhibited the highest performance in two of three  
457 catchments (405219 and 405264), followed successively by scenario 3, scenario 2,  
458 and scenario 1. During the verification period, the median  $NSE_{\text{sqrt}}$  performance in  
459 scenario 4 was 0.80% higher than scenario 5, however, the variation range in scenario  
460 4 was 53% wider than the latter. These results demonstrate that the time-varying  
461 scheme (scenario 4) for model parameters improved the median  $NSE_{\text{sqrt}}$  performance  
462 but also amplified the projection uncertainty compared with the results from the  
463 stationary scheme (scenario 5) for model parameters. In the DSST scheme of  
464 calibrating in the dry years and verifying in the wet years, scenario 3, which  
465 considered both spatial coherence of  $\beta$  and  $\omega$  between different catchments,  
466 exhibited the highest median  $NSE_{\text{sqrt}}$  for all catchments, had the smallest fluctuation  
467 range in two catchments (225219 and 405264) and is the second smallest scenario in  
468 variation in catchment 40519 during the verification period. Conversely, scenario 2,  
469 the scenario with the best median estimate performance during the verification period  
470 in Figure 5, is just the fourth in all five scenarios in this DSST scheme. Compared  
471 with other model scenarios, the incorporation of spatial coherence of both regression  
472 parameters in scenario 3 reduced the projection uncertainty and improved the  
473 robustness of the model performance, with the smallest fluctuation ranges in most  
474 options under the contrasting climatic conditions. It indicates that the spatial setting of  
475 model parameters between different catchments provided a clear input for reducing  
476 the uncertainty of the model projection performance during the verification period. In  
477 addition, it also should be noted that model parameters calibrated over dry years,

478 contrastively, were not suitable for predicting runoff over wet years because of a  
479 larger degradation in projection performance than the scheme with the adverse  
480 calibration-verification direction.

481 Comparing the DIC results for both DSST schemes in Table 4 and Table 5, the  
482 best DIC value is achieved by scenario 3, which incorporates the spatial coherence of  
483 both regression parameters and is the most complex scenario in the comparison. This  
484 finding is consistent with the results by the  $NSE_{\text{sqrt}}$  criterion and showed the validity  
485 of the spatial coherence of both regression parameters in ensuring the robustness of  
486 the hydrological projection performance. In addition, when [comparing](#) DIC results of  
487 scenarios 4 and 5, the setting of time-varying functions improved the DIC  
488 performance in both DSST schemes. This finding also agreed with the results by the  
489  $NSE_{\text{sqrt}}$  criterion and indicated the positive implications of the time-varying model  
490 parameters on the projection performance.

491 Tables 6 and 7 illustrate the performance of high and low flows during the  
492 verification period in terms of MaxF and MinF estimates for the median projected  
493 streamflows in both DSST schemes. As shown in table 7, for the projection of high  
494 flow part, scenario 3 exhibits the best performance in all catchments among five  
495 scenarios under the scheme of calibrating in the dry years and verifying in the wet  
496 years. For the projection performance in the other DSST scheme (Table 6), scenario 3  
497 has the best projection performance in high flow part in catchment 225219 and is the  
498 second-best scenario in the other two catchments. It indicates that the incorporation of  
499 spatial coherence of both [amplitude](#)  $\beta$  and [frequency](#)  $\omega$  successfully improves

500 the projection performance in the high flow part. As for the projection of the low flow  
501 part, the discrepancy between the results of different scenarios and the observed low  
502 flows is not obvious (The absolute differences between the observed values and  
503 modeled values are very small). Furthermore, scenario 3 shows the best-projected  
504 performance in two catchments (405219 and 405264) in the scheme of calibrating in  
505 dry years and verifying in wet years, and is the best scenario in catchment 405264 in  
506 the scheme of calibrating in wet years and verifying in dry years. In addition, scenario  
507 3 is the second-best option in catchments 225219 and 405219 under the scheme of  
508 calibrating in wet years and verifying in dry years. Combined with the projection  
509 performance of both high and low flows, scenario 3 achieves its superior projection  
510 performance mainly by the improvement in the prediction of high flow parts.

511 Figure 7 shows the BIAS estimates for the median of the posterior distribution of  
512 model parameters for all modeling scenarios across all catchments when  
513 transferability between the [wet and dry years](#) was examined. Although the BIAS was  
514 a component of the objective function (Eq. 3), the 10-year rolling average BIAS still  
515 deviated considerably from a value of 1 for all the scenarios in the two DSST schemes.  
516 The median estimates of the posterior distribution in both scenarios performed well in  
517 the  $NSE_{\text{sqrt}}$  criterion for both periods. However, the median estimates did not ensure  
518 unbiased simulations over the modeling period; one scenario with a higher  $NSE_{\text{sqrt}}$   
519 criterion may have an altered BIAS during the modeling period. The BIAS results in  
520 catchments 225219 and 405219 showed some similarity: all scenarios tended to  
521 underestimate streamflow along the time sequence in both DSST schemes. Conversely,



522 all scenarios tended to overestimate the streamflow in catchment 405264 in both  
523 schemes. By comparing the BIAS performance for the five scenarios, it was observed  
524 that the spatial setting of modeling scenarios generally tended to enlarge the BIAS in  
525 all catchments, while the difference between scenarios 4 and 5 was very small.

### 526 **4.3 Parameter uncertainty analysis**

527 The uncertainty of the parameters was characterized by the posterior distribution  
528 of the regression parameters and was derived by the MCMC iteration. As mentioned  
529 in section 2.3.2, **amplitude  $\beta$**  and **frequency  $\omega$**  were assumed to have different  
530 levels of spatial coherence in each modeling scenario (Table 1); these scenarios in  
531 each DSST regime are compared in Figs. 8 and 9. It should be mentioned that there  
532 was no regression parameter in scenario 5. Solid lines in the violin plots represent the  
533 25<sup>th</sup> and 75<sup>th</sup> percentiles of the posterior distribution. **The white dots in the violin plot**  
534 **denote the median estimate of the posterior distribution.** In the upper plots in Figures  
535 8 and 9, it can be clearly seen that the first three scenarios had a much smaller  
536 variation interval than scenario 4 in terms of amplitude  $\beta$ , which denotes the  
537 amplitude of the sine function. The catchment averages of both schemes of the  
538 median estimates of  $\beta$  in the first three scenarios are 2.78, -4.91, and 9.26  
539 respectively, while that in the fourth scenario is much larger, reached at -39.20.  
540 Scenario 3, which considered both spatial coherence of amplitude  $\beta$  and frequency  
541  $\omega$ , has the narrowest interval of  $\beta$  for all catchments, followed successively by  
542 scenario 1 (only considered the spatial coherence of the amplitude  $\beta$ ), scenario 2  
543 (only frequency  $\omega$  was spatially coherent), and scenario 4 (no regression parameter

544 was spatially coherent). With regards to the regression parameter  $\omega$ , which denotes  
545 the frequency of the sine function (in the lower figures of Figures 8 and 9), its median  
546 estimates in both four scenarios differ slightly. As shown in Figure 8, the catchment  
547 averages of frequency  $\omega$  for different scenarios are 0.24, 0.14, 0.15, and 0.18, while  
548 those in Figure 9 are 0.15, 0.26, 0.23, and 0.17 respectively. The period  $T$  of the sine  
549 term could be derived based on the estimates of  $\omega$  by equation  $T = 2\pi/\omega$ . Thus,  
550 the mean periods  $T$  of model parameter  $\theta_1$  for different scenarios are 26.2, 46.3,  
551 41.9 and 35.2 in Figure 8, respectively. Similarly, the mean periods  $T$  are 42.9, 24.1,  
552 27.4 and 38.0 in Figure 9, respectively. In addition, we used the Hilbert-Huang  
553 Transform method (Huang et al., 1998) to identify the potential periods of the series  
554 of several climate variables (including the daily rainfall, daily potential  
555 evapotranspiration, daily maximum temperature and daily minimum temperature in  
556 the studied catchments). It was found that these daily series have periods of 22.2~49.1  
557 days. Thus, we guess that the potential periods of these climate variables may be the  
558 possible reasons for the periods of time-varying parameters. It also should be  
559 mentioned that the adopted Hilbert spectrum method is one of the most popular  
560 methods for analyzing nonlinear and non-stationary data. Huang et al. (1999)  
561 indicated that this method is better than the Fourier transform method and Wavelet  
562 Transform method in processing nonlinear and non-stationary data.

563 In summary, by combining the results of parameter uncertainty estimation and  
564 model projection performance evaluation, the incorporation of spatial coherence  
565 successfully improved the robustness of the projection performance in both DSST

566 schemes by controlling the estimation uncertainty of amplitude  $\beta$ .

## 567 **5. CONCLUSIONS**

568 In this study, a two-level HB framework was used to incorporate the spatial  
569 coherence of adjacent catchments to improve the hydrological projection performance  
570 of sensitive time-varying parameters for a lumped conceptual rainfall-runoff model  
571 (GR4J) under contrasting climatic conditions. Firstly, a temporal parameter transfer  
572 scheme was implemented, using a DSST procedure in which the available data were  
573 divided into wet and dry years. Then, the model was calibrated in the wet years and  
574 evaluated in the dry years, and vice versa. In the first level of the proposed HB  
575 framework, the most sensitive parameter in the GR4J model, i.e., the production  
576 storage capacity ( $\theta_1$ ), was allowed to vary with time to account for the periodic  
577 variation that had significant impacts on the extensionality of the model. The periodic  
578 variation in catchment storage capacity was represented by a sine function for  $\theta_1$   
579 (parameterized by amplitude and frequency). In the second level, four modeling  
580 scenarios with different spatial coherence schemes, and one scenario with a stationary  
581 scheme of catchment storage capacity, were used to evaluate the transferability of  
582 hydrological models under contrasting climatic conditions. Finally, the proposed  
583 method was applied to three spatially adjacent, unregulated, and unimpaired  
584 catchments in southeast Australia. The study concludes that: (1) the time-varying  
585 setting was valid in improving the model performance but also extended the  
586 projection uncertainty in contrast to the stationary setting; (2) the inclusion of spatial  
587 coherence successfully reduced the projection uncertainty and improved the

588 robustness of model performance; and (3) a large performance degradation has been  
589 found in the DSST scheme with its model parameters calibrated over dry years and  
590 verified in the wet years. This study improves our understanding of the spatial  
591 coherence of time-varying parameters, which will help improve the projection  
592 performance under differing climatic conditions. However, there are several unsolved  
593 problems that need to be addressed. First, the spatial setting of regression parameters  
594 may expand the BIAS between the simulation and streamflow observation with a  
595 single objective function; the potential physical mechanism behind this result should  
596 be explored further. Secondly, this study was confined to spatially coherent  
597 catchments that are similar in climatic and hydrogeological conditions; further  
598 research is needed to determine which factors have the most significant impacts on  
599 model projection performance when considering obvious inputs from other  
600 catchments.

601

## 602 **ACKNOWLEDGMENTS**

603 This study was supported by the National Key Research and Development  
604 Program (2018YFC0407202), the National Natural Science Foundation of China  
605 (51861125102; 51879193), the Natural Science Foundation of Hubei Province  
606 (2017CFA015), and the Research Council of Norway (FRINATEK Project 274310).  
607 The numerical calculations were done on the supercomputing system in the  
608 Supercomputing Center of Wuhan University. The authors would like to thank the  
609 editor and anonymous reviewers for their comments, which helped improve the

610 quality of the paper.

## 611 **AUTHOR CONTRIBUTIONS**

612 All of the authors helped to conceive and design the analysis. Zhengke Pan and  
613 Pan Liu performed the analysis and wrote the paper. Shida Gao, Jun Xia, Jie Chen,  
614 and Lei Cheng contributed to the writing of the paper and made comments.

## 615 **COMPLIANCE WITH ETHICAL STANDARDS**

616 **Conflict of interest:** The authors declare that they have no conflict of interest.

## 617 **REFERENCES**

- 618 Ajami, N. K., Duan, Q. Y., and Sorooshian, S.: An integrated hydrologic Bayesian multimodel  
619 combination framework: Confronting input, parameter, and model structural uncertainty in  
620 hydrologic prediction, *Water Resour. Res.*, 43, 10.1029/2005wr004745, 2007.
- 621 Bracken, C., Holman, K. D., Rajagopalan, B., and Moradkhani, H.: A Bayesian Hierarchical  
622 Approach to Multivariate Nonstationary Hydrologic Frequency Analysis, *Water Resour. Res.*,  
623 54, 243-255, 10.1002/2017wr020403, 2018.
- 624 Brigode, P., Oudin, L., and Perrin, C.: Hydrological model parameter instability: A source of  
625 additional uncertainty in estimating the hydrological impacts of climate change?, *J. Hydrol.*,  
626 476, 410-425, 10.1016/j.jhydrol.2012.11.012, 2013.
- 627 Broderick, C., Matthews, T., Wilby, R. L., Bastola, S., and Murphy, C.: Transferability of  
628 hydrological models and ensemble averaging methods between contrasting climatic periods,  
629 *Water Resour. Res.*, 52, 8343-8373, 10.1002/2016wr018850, 2016.
- 630 Cha, Y., Park, S. S., Lee, H. W., and Stow, C. A.: A Bayesian hierarchical approach to model  
631 seasonal algal variability along an upstream to downstream river gradient, *Water Resour.*  
632 *Res.*, 52, 348-357, 10.1002/2015wr017327, 2016.
- 633 Chen, X., Hao, Z., Devineni, N., and Lall, U.: Climate information based streamflow and  
634 rainfall forecasts for Huai River basin using hierarchical Bayesian modeling, *Hydrol. Earth Syst.*  
635 *Sci.*, 18, 1539-1548, 10.5194/hess-18-1539-2014, 2014.
- 636 Chiew, F. H. S., Teng, J., Vaze, J., Post, D. A., Perraud, J. M., Kirono, D. G. C., and Viney, N. R.:  
637 Estimating climate change impact on runoff across southeast Australia: Method, results, and  
638 implications of the modeling method, *Water Resour. Res.*, 45, 17, 10.1029/2008wr007338,  
639 2009.
- 640 Chiew, F. H. S., Potter, N. J., Vaze, J., Petheram, C., Zhang, L., Teng, J., and Post, D. A.:  
641 Observed hydrologic non-stationarity in far south-eastern Australia: implications for  
642 modelling and prediction, *Stoch. Environ. Res. Risk Assess.*, 28, 3-15,  
643 10.1007/s00477-013-0755-5, 2014.

644 Ciais, P., Reichstein, M., Viovy, N., Granier, A., Ogee, J., Allard, V., Aubinet, M., Buchmann, N.,  
645 Bernhofer, C., Carrara, A., Chevallier, F., De Noblet, N., Friend, A. D., Friedlingstein, P.,  
646 Grunwald, T., Heinesch, B., Keronen, P., Knohl, A., Krinner, G., Loustau, D., Manca, G.,  
647 Matteucci, G., Miglietta, F., Ourcival, J. M., Papale, D., Pilegaard, K., Rambal, S., Seufert, G.,  
648 Soussana, J. F., Sanz, M. J., Schulze, E. D., Vesala, T., and Valentini, R.: Europe-wide reduction  
649 in primary productivity caused by the heat and drought in 2003, *Nature*, 437, 529-533,  
650 10.1038/nature03972, 2005.

651 Clarke, R. T.: Hydrological prediction in a non-stationary world, *Hydrol. Earth Syst. Sci.*, 11,  
652 408-414, 10.5194/hess-11-408-2007, 2007.

653 Cook, E. R., Woodhouse, C. A., Eakin, C. M., Meko, D. M., and Stahle, D. W.: Long-term aridity  
654 changes in the western United States, *Science*, 306, 1015-1018, 10.1126/science.1102586,  
655 2004.

656 Cooley, D., Nychka, D., and Naveau, P.: Bayesian spatial modeling of extreme precipitation  
657 return levels, *J. Am. Stat. Assoc.*, 102, 824-840, 10.1198/016214506000000780, 2007.

658 Coron, L., Andreassian, V., Perrin, C., Lerat, J., Vaze, J., Bourqui, M., and Hendrickx, F.: Crash  
659 testing hydrological models in contrasted climate conditions: An experiment on 216  
660 Australian catchments, *Water Resour. Res.*, 48, 17, 10.1029/2011wr011721, 2012.

661 Deng, C., Liu, P., Guo, S. L., Li, Z. J., and Wang, D. B.: Identification of hydrological model  
662 parameter variation using ensemble Kalman filter, *Hydrol. Earth Syst. Sci.*, 20, 4949-4961,  
663 10.5194/hess-20-4949-2016, 2016.

664 Deng, C., Liu, P., Wang, D. B., and Wang, W. G.: Temporal variation and scaling of parameters  
665 for a monthly hydrologic model, *J. Hydrol.*, 558, 290-300, 10.1016/j.jhydrol.2018.01.049,  
666 2018.

667 Duan, Q. Y., Ajami, N. K., Gao, X. G., and Sorooshian, S.: Multi-model ensemble hydrologic  
668 prediction using Bayesian model averaging, *Adv. Water Resour.*, 30, 1371-1386,  
669 10.1016/j.advwatres.2006.11.014, 2007.

670 Ekstrom, M., Gutmann, E. D., Wilby, R. L., Tye, M. R., and Kirono, D. G. C.: Robustness of  
671 hydroclimate metrics for climate change impact research, *Wiley Interdiscip. Rev.-Water*, 5, 20,  
672 10.1002/wat2.1288, 2018.

673 Fowler, K. J. A., Peel, M. C., Western, A. W., Zhang, L., and Peterson, T. J.: Simulating runoff  
674 under changing climatic conditions: Revisiting an apparent deficiency of conceptual  
675 rainfall-runoff models, *Water Resour. Res.*, 52, 1820-1846, 10.1002/2015wr018068, 2016.

676 Gelman, A., Carlin, J., Stern, H., Dunson, D., Vehtari, A., and Rubin, D.: *Bayesian Data Analysis*,  
677 third ed ed., CRC Press, 2013.

678 Guo, D. L., Westra, S., and Maier, H. R.: Impact of evapotranspiration process representation  
679 on runoff projections from conceptual rainfall-runoff models, *Water Resour. Res.*, 53,  
680 435-454, 10.1002/2016wr019627, 2017.

681 Heuvelmans, G., Muys, B., and Feyen, J.: Regionalisation of the parameters of a hydrological  
682 model: Comparison of linear regression models with artificial neural nets, *J. Hydrol.*, 319,  
683 245-265, 10.1016/j.jhydrol.2005.07.030, 2006.

684 Huang, N. E., Shen, Z., Long, S. R., Wu, M. L. C., Shih, H. H., Zheng, Q. N., Yen, N. C., Tung, C.  
685 C., and Liu, H. H.: The empirical mode decomposition and the Hilbert spectrum for nonlinear  
686 and non-stationary time series analysis, *Proc. R. Soc. A-Math. Phys. Eng. Sci.*, 454, 903-995,  
687 10.1098/rspa.1998.0193, 1998.

688 Huang, N. E., Shen, Z., and Long, S. R.: A new view of nonlinear water waves: The Hilbert  
689 spectrum, *Annu. Rev. Fluid Mech.*, 31, 417-457, 10.1146/annurev.fluid.31.1.417, 1999.

690 Lebecherel, L., Andreassian, V., and Perrin, C.: On evaluating the robustness of  
691 spatial-proximity-based regionalization methods, *J. Hydrol.*, 539, 196-203,  
692 10.1016/j.jhydrol.2016.05.031, 2016.

693 Lima, C. H. R., and Lall, U.: Hierarchical Bayesian modeling of multisite daily rainfall  
694 occurrence: Rainy season onset, peak, and end, *Water Resour. Res.*, 45, 14,  
695 10.1029/2008wr007485, 2009.

696 Lima, C. H. R., Lall, U., Troy, T., and Devineni, N.: A hierarchical Bayesian GEV model for  
697 improving local and regional flood quantile estimates, *J. Hydrol.*, 541, 816-823,  
698 10.1016/j.jhydrol.2016.07.042, 2016.

699 Liu, P., Li, L. P., Chen, G. J., and Rheinheimer, D. E.: Parameter uncertainty analysis of reservoir  
700 operating rules based on implicit stochastic optimization, *J. Hydrol.*, 514, 102-113,  
701 10.1016/j.jhydrol.2014.04.012, 2014.

702 Liu, Y. Q., and Gupta, H. V.: Uncertainty in hydrologic modeling: Toward an integrated data  
703 assimilation framework, *Water Resour. Res.*, 43, 18, 10.1029/2006wr005756, 2007.

704 Merz, R., and Blöschl, G.: Regionalisation of catchment model parameters, *J. Hydrol.*, 287,  
705 95-123, 10.1016/j.jhydrol.2003.09.028, 2004.

706 Merz, R., Parajka, J., and Blöschl, G.: Time stability of catchment model parameters:  
707 Implications for climate impact analyses, *Water Resour. Res.*, 47, 17, 10.1029/2010wr009505,  
708 2011.

709 Moore, R. D., and Wondzell, S. M.: Physical hydrology and the effects of forest harvesting in  
710 the Pacific Northwest: A review, *J. Am. Water Resour. Assoc.*, 41, 763-784, 2005.

711 Moradkhani, H., Hsu, K. L., Gupta, H., and Sorooshian, S.: Uncertainty assessment of  
712 hydrologic model states and parameters: Sequential data assimilation using the particle filter,  
713 *Water Resour. Res.*, 41, 17, 10.1029/2004wr003604, 2005.

714 Moradkhani, H., DeChant, C. M., and Sorooshian, S.: Evolution of ensemble data assimilation  
715 for uncertainty quantification using the particle filter-Markov chain Monte Carlo method,  
716 *Water Resour. Res.*, 48, 13, 10.1029/2012wr012144, 2012.

717 Moriasi, D. N., Arnold, J. G., Van Liew, M. W., Bingner, R. L., Harmel, R. D., and Veith, T. L.:  
718 Model evaluation guidelines for systematic quantification of accuracy in watershed  
719 simulations, *Trans. ASABE*, 50, 885-900, 2007.

720 Najafi, M. R., and Moradkhani, H.: A hierarchical Bayesian approach for the analysis of  
721 climate change impact on runoff extremes, *Hydrol. Process.*, 28, 6292-6308,  
722 10.1002/hyp.10113, 2014.

723 Nash, J. E., and Sutcliffe, J. V.: River flow forecasting through conceptual models part I — A  
724 discussion of principles, *J. Hydrol.*, 10, 282-290,  
725 [https://doi.org/10.1016/0022-1694\(70\)90255-6](https://doi.org/10.1016/0022-1694(70)90255-6), 1970.

726 Oudin, L., Andreassian, V., Perrin, C., Michel, C., and Le Moine, N.: Spatial proximity, physical  
727 similarity, regression and ungaged catchments: A comparison of regionalization approaches  
728 based on 913 French catchments, *Water Resour. Res.*, 44, 15, 10.1029/2007wr006240, 2008.

729 Pan, Z., Liu, P., Gao, S., Cheng, L., Chen, J., and Zhang, X.: 1Reducing the uncertainty of  
730 time-varying hydrological model parameters using spatial coherence within a hierarchical  
731 Bayesian framework, *J. Hydrol.*, 10.1016/j.jhydrol.2019.123927, 2019.

732 Pathiraja, S., Marshall, L., Sharma, A., and Moradkhani, H.: Detecting non-stationary  
733 hydrologic model parameters in a paired catchment system using data assimilation, *Adv.*  
734 *Water Resour.*, 94, 103-119, 10.1016/j.advwatres.2016.04.021, 2016.

735 Pathiraja, S., Moradkhani, H., Marshall, L., Sharma, A., and Geenens, G.: Data-Driven Model  
736 Uncertainty Estimation in Hydrologic Data Assimilation, *Water Resour. Res.*, 54, 1252-1280,  
737 10.1002/2018wr022627, 2018.

738 Patil, S. D., and Stieglitz, M.: Comparing Spatial and temporal transferability of hydrological  
739 model parameters, *J. Hydrol.*, 525, 409-417, 10.1016/j.jhydrol.2015.04.003, 2015.

740 Perrin, C., Michel, C., and Andreassian, V.: Improvement of a parsimonious model for  
741 streamflow simulation, *J. Hydrol.*, 279, 275-289, 10.1016/s0022-1694(03)00225-7, 2003.

742 Renard, B., Kavetski, D., Leblois, E., Thyer, M., Kuczera, G., and Franks, S. W.: Toward a reliable  
743 decomposition of predictive uncertainty in hydrological modeling: Characterizing rainfall  
744 errors using conditional simulation, *Water Resour. Res.*, 47, 21, 10.1029/2011wr010643,  
745 2011.

746 Saft, M., Western, A. W., Zhang, L., Peel, M. C., and Potter, N. J.: The influence of multiyear  
747 drought on the annual rainfall-runoff relationship: An Australian perspective, *Water Resour.*  
748 *Res.*, 51, 2444-2463, 10.1002/2014wr015348, 2015.

749 Seiller, G., Anctil, F., and Perrin, C.: Multimodel evaluation of twenty lumped hydrological  
750 models under contrasted climate conditions, *Hydrol. Earth Syst. Sci.*, 16, 1171-1189,  
751 10.5194/hess-16-1171-2012, 2012.

752 Singh, S. K., Bardossy, A., Gotzinger, J., and Sudheer, K. P.: Effect of spatial resolution on  
753 regionalization of hydrological model parameters, *Hydrol. Process.*, 26, 3499-3509,  
754 10.1002/hyp.8424, 2012.

755 Spiegelhalter, D. J., Best, N. G., Carlin, B. R., and van der Linde, A.: Bayesian measures of  
756 model complexity and fit, *J. R. Stat. Soc. Ser. B-Stat. Methodol.*, 64, 583-616,  
757 10.1111/1467-9868.00353, 2002.

758 Sun, X., Thyer, M., Renard, B., and Lang, M.: A general regional frequency analysis framework  
759 for quantifying local-scale climate effects: A case study of ENSO effects on Southeast  
760 Queensland rainfall, *J. Hydrol.*, 512, 53-68, 10.1016/j.jhydrol.2014.02.025, 2014.

761 Sun, X., and Lall, U.: Spatially coherent trends of annual maximum daily precipitation in the  
762 United States, *Geophys. Res. Lett.*, 42, 9781-9789, 10.1002/2015gl066483, 2015.

763 Sun, X., Lall, U., Merz, B., and Dung, N. V.: Hierarchical Bayesian clustering for nonstationary  
764 flood frequency analysis: Application to trends of annual maximum flow in Germany, *Water*  
765 *Resour. Res.*, 51, 6586-6601, 10.1002/2015wr017117, 2015.

766 Tegegne, G., and Kim, Y. O.: Modelling ungauged catchments using the catchment runoff  
767 response similarity, *J. Hydrol.*, 564, 452-466, 10.1016/j.jhydrol.2018.07.042, 2018.

768 Vaze, J., Post, D. A., Chiew, F. H. S., Perraud, J. M., Viney, N. R., and Teng, J.: Climate  
769 non-stationarity - Validity of calibrated rainfall-runoff models for use in climate change  
770 studies, *J. Hydrol.*, 394, 447-457, 10.1016/j.jhydrol.2010.09.018, 2010.

771 Vrugt, J. A., Gupta, H. V., Bouten, W., and Sorooshian, S.: A Shuffled Complex Evolution  
772 Metropolis algorithm for optimization and uncertainty assessment of hydrologic model  
773 parameters, *Water Resour. Res.*, 39, 18, 10.1029/2002wr001642, 2003.

774 Vrugt, J. A., ter Braak, C. J. F., Diks, C. G. H., Robinson, B. A., Hyman, J. M., and Higdon, D.:  
775 Accelerating Markov Chain Monte Carlo Simulation by Differential Evolution with



776 Self-Adaptive Randomized Subspace Sampling, *International Journal of Nonlinear Sciences*  
777 *and Numerical Simulation*, 10, 273-290, 2009.

778 Westra, S., Thyer, M., Leonard, M., Kavetski, D., and Lambert, M.: A strategy for diagnosing  
779 and interpreting hydrological model nonstationarity, *Water Resour. Res.*, 50, 5090-5113,  
780 10.1002/2013wr014719, 2014.

781 Wright, D. P., Thyer, M., and Westra, S.: Influential point detection diagnostics in the context  
782 of hydrological model calibration, *J. Hydrol.*, 527, 1161-1172, 10.1016/j.jhydrol.2015.05.047,  
783 2015.

784 Xiong, M., Liu, P., Cheng, L., Deng, C., Gui, Z., Zhang, X., and Liu, Y.: Identifying time-varying  
785 hydrological model parameters to improve simulation efficiency by the ensemble Kalman  
786 filter: A joint assimilation of streamflow and actual evapotranspiration, *J. Hydrol.*, 568,  
787 758-768, 10.1016/j.jhydrol.2018.11.038, 2019.

788 Xu, Q., Chen, J., Peart, M. R., Ng, C. N., Hau, B. C. H., and Law, W. W. Y.: Exploration of  
789 severities of rainfall and runoff extremes in ungauged catchments: A case study of Lai Chi Wo  
790 in Hong Kong, China, *Sci. Total Environ.*, 634, 640-649, 10.1016/j.scitotenv.2018.04.024,  
791 2018.

792 Yan, H. X., and Moradkhani, H.: A regional Bayesian hierarchical model for flood frequency  
793 analysis, *Stoch. Environ. Res. Risk Assess.*, 29, 1019-1036, 10.1007/s00477-014-0975-3, 2015.

794 Zhang, X. J., Liu, P., Cheng, L., Liu, Z. J., and Zhao, Y.: A back-fitting algorithm to improve  
795 real-time flood forecasting, *J. Hydrol.*, 562, 140-150, 10.1016/j.jhydrol.2018.04.051, 2018.

796 Zhang, Y. Q., Viney, N., Frost, A., and Oke, A.: Collation of Australian modeller's streamflow  
797 dataset for 780 unregulated Australian catchments, *Water for a healthy country national*  
798 *research flagship*, 115pp, 2013.

799

800 **TABLES**

801 **Table 1. Different spatial coherence scenarios for amplitude  $\beta$  and frequency  $\omega$  in the time-varying functional form of model parameter**  
 802  **$\theta_1$ . To explore the performance of spatial coherence within the time-varying function, different levels of spatial coherence for amplitude**  
 803  **$\beta$  and frequency  $\omega$  were assumed for the first three scenarios; in contrast, no spatial coherence is assumed in scenario 4, and a**  
 804 **temporally stable  $\theta_1$  is assumed in scenario 5.**

Category	Scenario	$\beta$	$\omega$	Constraints
Time-varying Spatial coherence	1	Parameter $\beta$ is region-related	Parameter $\omega$ is catchment-specific	$\theta_1 = \alpha(c) + \beta(c)\sin[\omega(c)t]$ , while $\beta(c) = N(\mu_2, \sigma_2^2)$
	2	Parameter $\beta$ is catchment-specific	Parameter $\omega$ is region-related	$\theta_1 = \alpha(c) + \beta(c)\sin[\omega(c)t]$ , while $\omega(c) = N(\mu_3, \sigma_3^2)$
	3	Parameter $\beta$ is region-related	Parameter $\omega$ is region-related	$\theta_1 = \alpha(c) + \beta(c)\sin[\omega(c)t]$ , while $\beta(c) = N(\mu_2, \sigma_2^2)$ and $\omega(c) = N(\mu_3, \sigma_3^2)$
Time invariant No spatial coherence	4	Parameter $\beta$ is catchment-specific	Parameter $\omega$ is catchment-specific	$\theta_1 = \alpha(c) + \beta(c)\sin[\omega(c)t]$
	5	No parameters $\beta$ or $\omega$		$\theta_1$ is stationary

805

806 NB:  $\theta_1$  represents the production storage capacity of the catchment;  $\beta$  is the slope describing long-term change during the modeling period, and  $\omega$  is the amplitude of  
 807 the sine function describing its seasonal variation during the modeling period;  $\mu_2, \sigma_2, \mu_3, \sigma_3$  are hyper-parameters.

808 **Table 2. Comparison of catchments attributes in terms of mean annual rainfall (mm), mean annual evaporation (mm), and mean annual**  
 809 **runoff (mm) for 1976–2011.**

810

Catchments ID	River Name	Observations start	Observations end	Mean annual rainfall	Mean annual potential evapotranspiration	Mean annual runoff
225219	Macalister	1/1/1976	30/12/2011	1064	1142	350
405219	Goulburn	1/1/1976	30/12/2011	1169	1193	422
405264	Big	1/1/1976	30/12/2011	1406	1157	469

811 **Table 3. Drought identification results for the catchments.**

812

Catchments ID	Drought start	Drought end	Length	Mean dry years anomaly	% Complete	R <sub>1</sub>	R <sub>2</sub>	Change in runoff (%)	Change in rainfall (%)
225219	1997	2009	12	-6.95%	90.4%	0.34	0.28	-15.98	-11.27
405219	1997	2009	12	-9.84%	98.5%	0.38	0.31	-18.57	-10.97
405264	1997	2009	12	-9.62%	98.5%	0.35	0.29	-18.23	-10.51

813 NB: R<sub>1</sub> and R<sub>2</sub> refer to the runoff coefficient during the wet and dry years, respectively.

814

815 **Table 4. Comparison of five scenarios in terms of the deviance information**  
 816 **criterion (DIC) when model parameters were calibrated in the wet years and**  
 817 **verified in the dry years.**

Category		Scenario	DIC
Time-varying	Spatial coherence	1	4961.7
		2	1202.3
		3	-1254.4
Time-invariant	No spatial coherence	4	5052.8
		5	5827.3

819

820 **Table 5. Comparison of five scenarios in terms of the deviance information**  
 821 **criterion (DIC) when model parameters were calibrated in the dry years and**  
 822 **verified in the wet years.**

Category		Scenario	DIC
Time-varying	Spatial coherence	1	-6167.0
		2	-5743.6
		3	-10574.0
Time-invariant	No spatial coherence	4	-8710.0
		5	-7460.8

824

825 **Table 6. Comparison of the projection performance of median flows during the**  
 826 **verification period associated with the Mean annual maximum flow (MaxF,**  
 827 **mm/d) and Mean annual minimum flow (MinF, mm/d) when model parameters**  
 828 **were calibrated in the wet years and verified in the dry years. The percentage**  
 829 **represents the % variation between the modeled value and the observed value.**

	Mean annual maximum flow			Mean annual minimum flow		
	225219	405219	405264	225219	405219	405264
Observed	10.58	11.98	9.23	0.050	0.093	0.17
Scenario 1	+25.7%	-52.9%	-27.7%	<b>+0.6%</b>	-51.3%	-25.6%
Scenario 2	-14.6%	<b>-14.6%</b>	-20.9%	+7.1%	-35.0%	-18.3%
Scenario 3	<b>+3.1%</b>	-36.1%	+5.6%	-17.9%	<b>-1.1%</b>	<b>-6.4%</b>
Scenario 4	-44.2%	-54.7%	<b>+3.3%</b>	+76.6%	-4.4%	-14.4%
Scenario 5	-52.1%	-49.7%	-13.6%	+72.0%	-6.9%	-29.1%

831

LNote:

832

1. The data in 1976 has been used for model warm-up to reduce the impact of the initial soil moisture conditions during the calibration period, and is not counted in the table;

833

834

2. The scenarios with bold values are labeled as the best scenario for projecting the streamflow during the verification periods, and the values from these scenarios have the least absolute

835

836

percentage difference with the observed values.

837

838 **Table 7. Comparison of the projection performance of median flows during the**  
839 **verification period associated with the Mean annual maximum flow (MaxF,**  
840 **mm/d) and Mean annual minimum flow (MinF, mm/d) when model parameters**  
841 **were calibrated in the dry years and verified in the wet years. The percentage**  
842 **represents the % variation between the modeled value and the observed value.**  
843

	Mean annual maximum flow			Mean annual minimum flow		
	225219	405219	405264	225219	405219	405264
Observed	10.73	12.06	8.94	0.03	0.09	0.19
Scenario 1	+15.5%	-43.1%	+44.3%	-26.5%	-51.1%	-52.4%
Scenario 2	+15.7%	-54.2%	+15.3%	-35.7%	<b>-29.8%</b>	-55.0%
Scenario 3	<b>+2.0%</b>	<b>-11.5%</b>	<b>-6.4%</b>	<b>-20.7%</b>	-41.4%	-50.0%
Scenario 4	+11.7%	-18.3%	+38.1%	-26.3%	-43.7%	<b>-49.5%</b>
Scenario 5	+32.2%	-21.6%	+34.0%	-42.8%	-45.1%	-50.0%

844

Note:

845

1. The data in 1997 has been used for model warm-up to reduce the impact of the initial soil moisture conditions during the calibration period, and is not counted in the table;

846

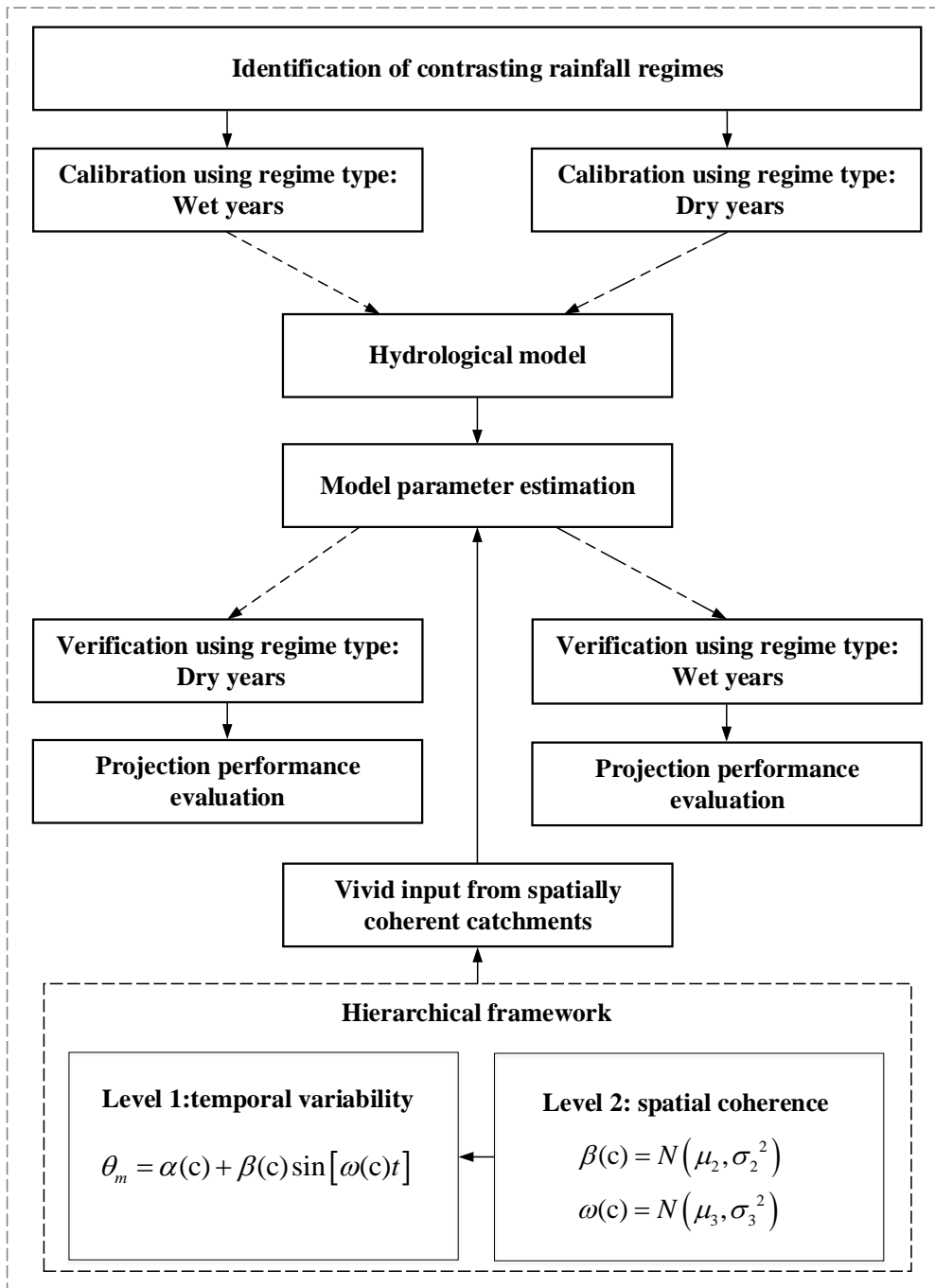
847

2. The scenarios with bold values are labeled as the best scenario for projecting the streamflow during the verification periods, and the values from these scenarios have the least absolute percentage difference with the observed values.

848

849

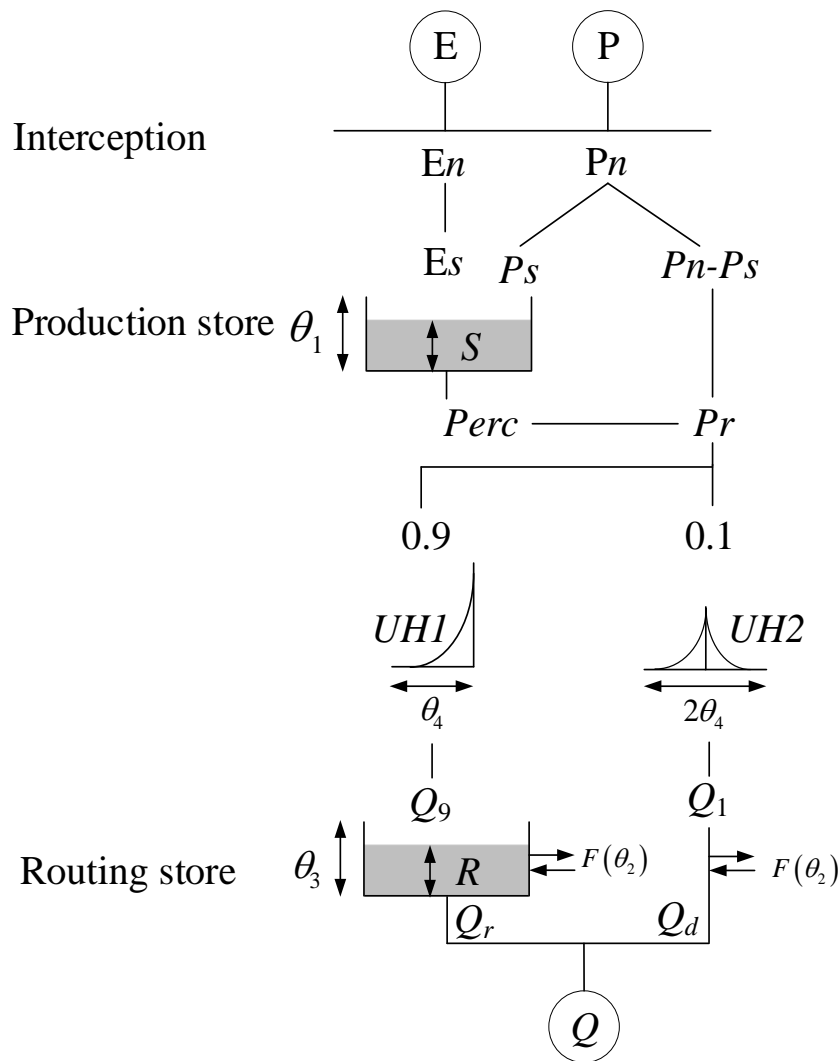
850



852

853 **Figure 1. Flow chart of the methodology for integrating inputs from spatially**  
 854 **coherent catchments and temporal variation of model parameters into a**  
 855 **hydrological model under contrasting climatic conditions (wet and dry years).**

856

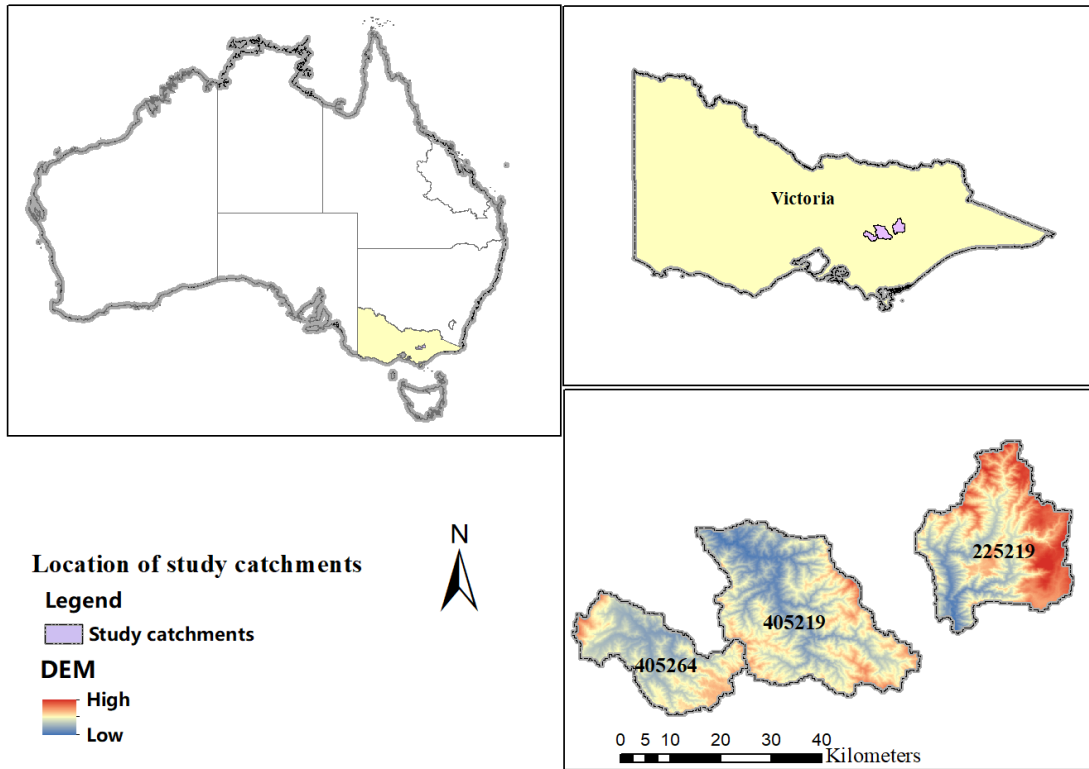


857

858 **Figure 2. Schematic diagram of the GR4J rainfall-runoff model adopted by**  
 859 **Perrin et al. (2003). In the figure, P and E refer to precipitation and**  
 860 **evapotranspiration, respectively;  $E_n$  and  $P_n$  denote net precipitation and net**  
 861 **evapotranspiration, respectively;  $P_s$  refers to the part of precipitation that fills**  
 862 **the production store (i.e.  $S$ ). The production store is determined as a function of**  
 863 **the water level  $S$  in the production store. The  $\theta_1, \theta_2, \theta_3$ , and  $\theta_4$  denote model**  
 864 **parameters. The  $Perc$  refers to the percolation leakage that is a function of**  
 865 **production store  $S$  and parameter  $\theta_1$ . The  $Pr$  refers to the total quantity of water**  
 866 **that reaches the routing functions. The  $UH1$  and  $UH2$  denote two unit**  
 867 **hydrographs. The  $Q_1$  and  $Q_9$  refer the corresponding output of the unit**  
 868 **hydrographs, respectively;  $F$  indicates the groundwater exchange term;  $R$  is the**  
 869 **level in the routing store. The  $Q_r$  refers to the outflow of the routing store,  $Q_d$  is a**  
 870 **function of water exchange, and  $Q$  refers to the total streamflow.**

871

872

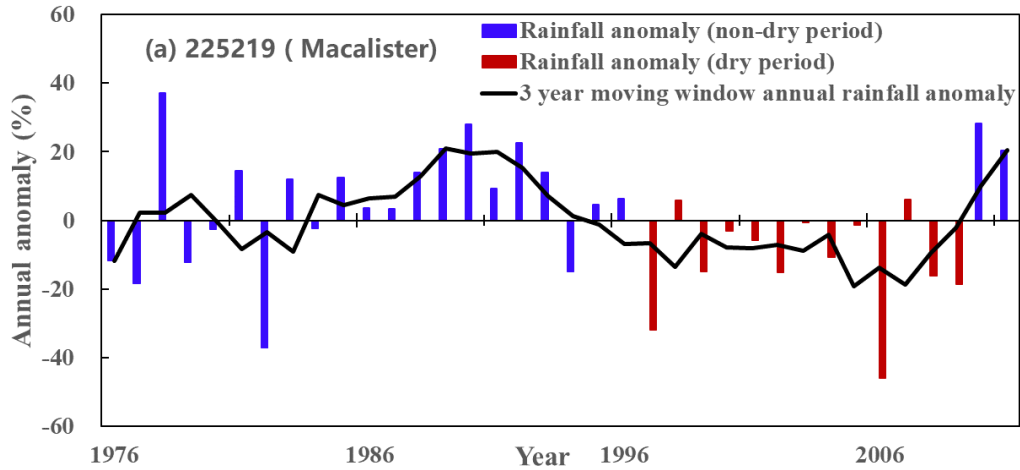


873  
874

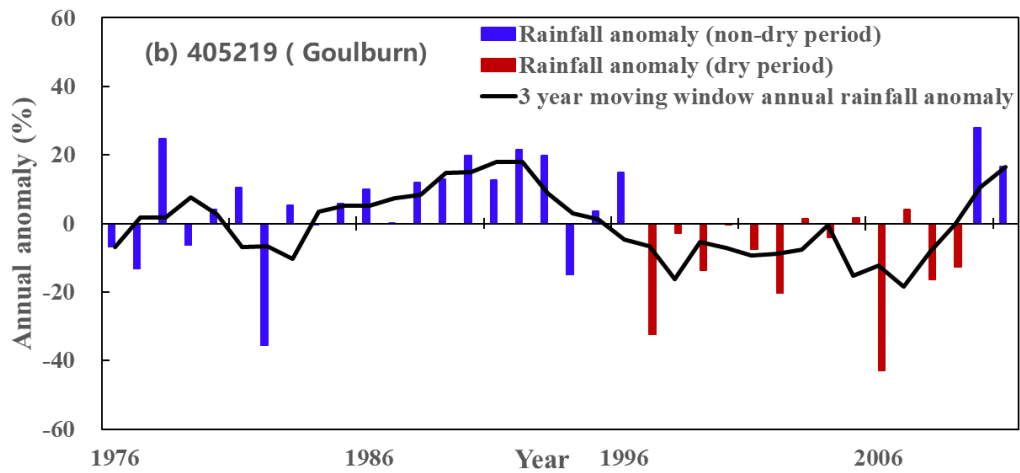
875 **Figure 3. Locations of study catchments in Victoria, Australia. The catchment**  
 876 **IDs are 225219 (Macalister River catchment), 405219 (Goulburn River**  
 877 **catchment), and 405264 (Big River catchment).**

878  
879  
880

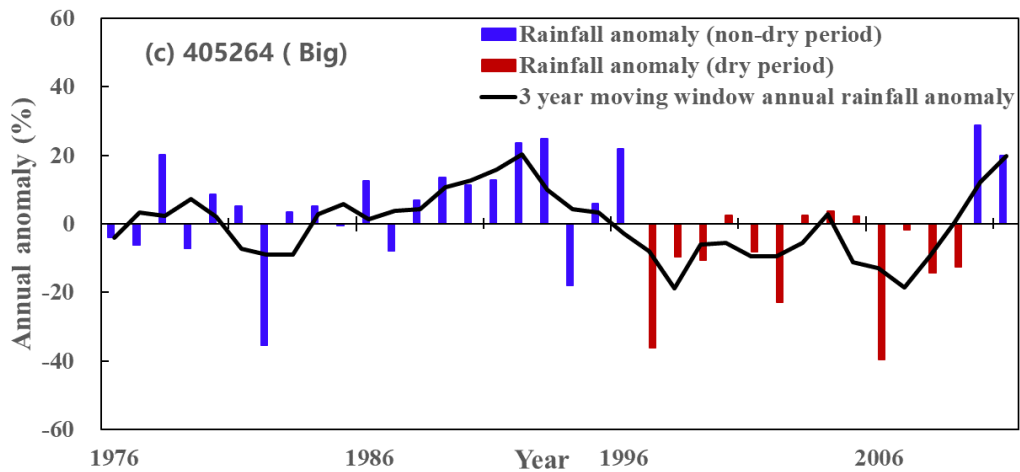




881

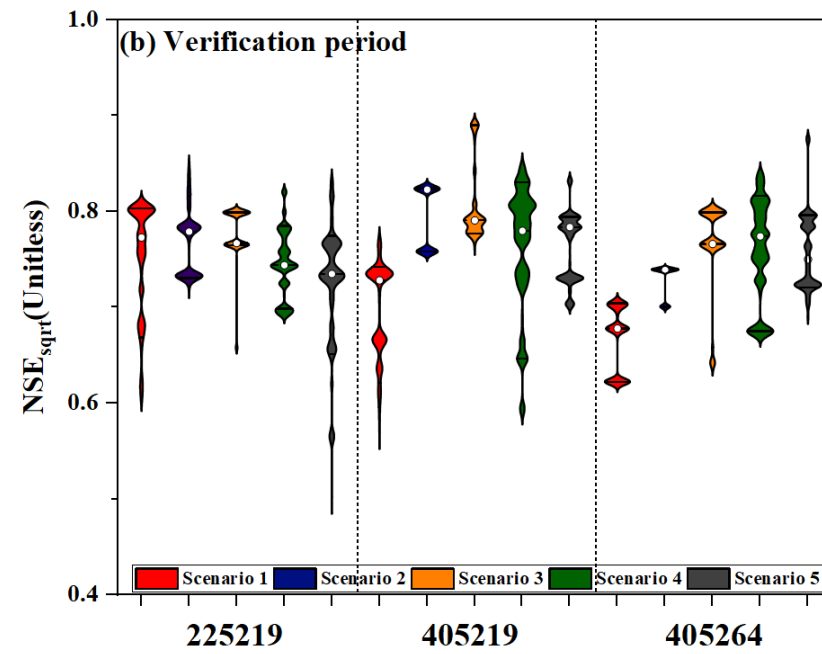
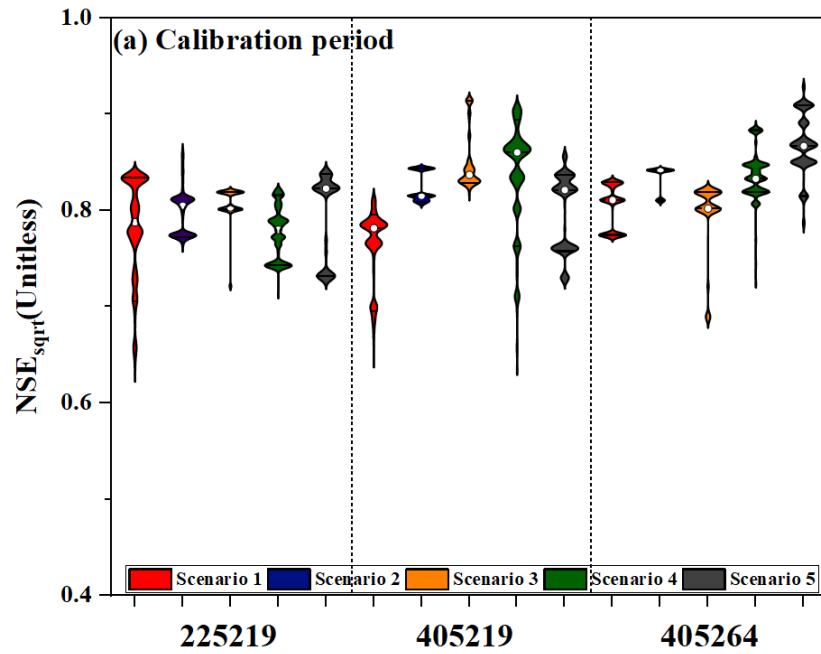


882

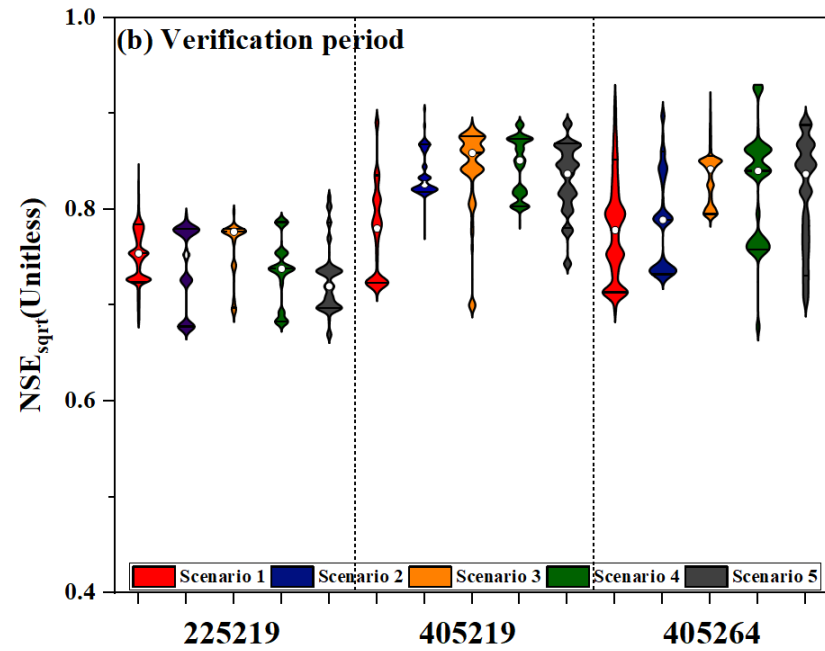
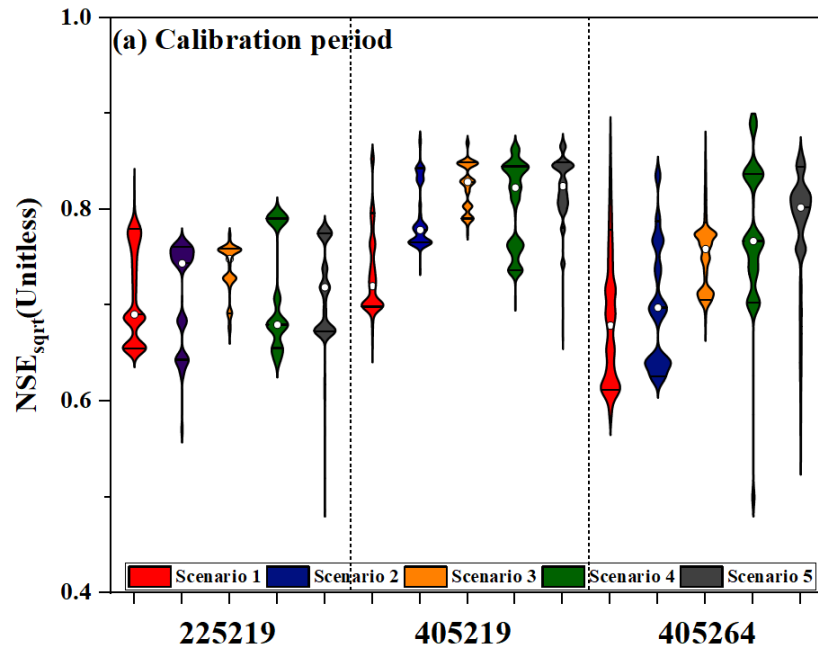


883

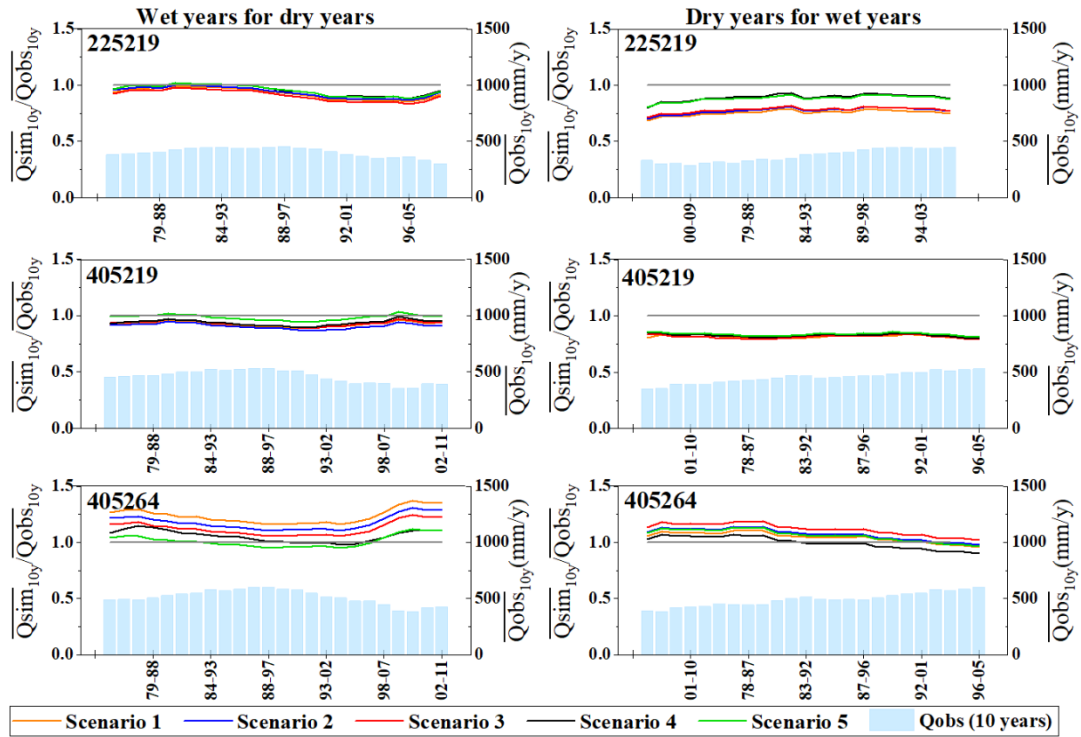
884 **Figure 4. The identified dry years in all catchments. The annual anomaly is**  
 885 **defined as a percentage of the mean annual rainfall**



886 **Figure 5.  $NSE_{\text{sqrt}}$  for each of the five scenarios for each catchment during (a) the calibration period (wet years) and (b) the verification**  
 887 **period (dry years). The white dots represent the median estimates of the results.**  
 888



889 **Figure 6.  $NSE_{\text{sqr}}$  for each of the five scenarios for each catchment during (a) the calibration period (dry years) and (b) the verification**  
 890 **period (wet years). The white dots represent the median estimates of the results.**

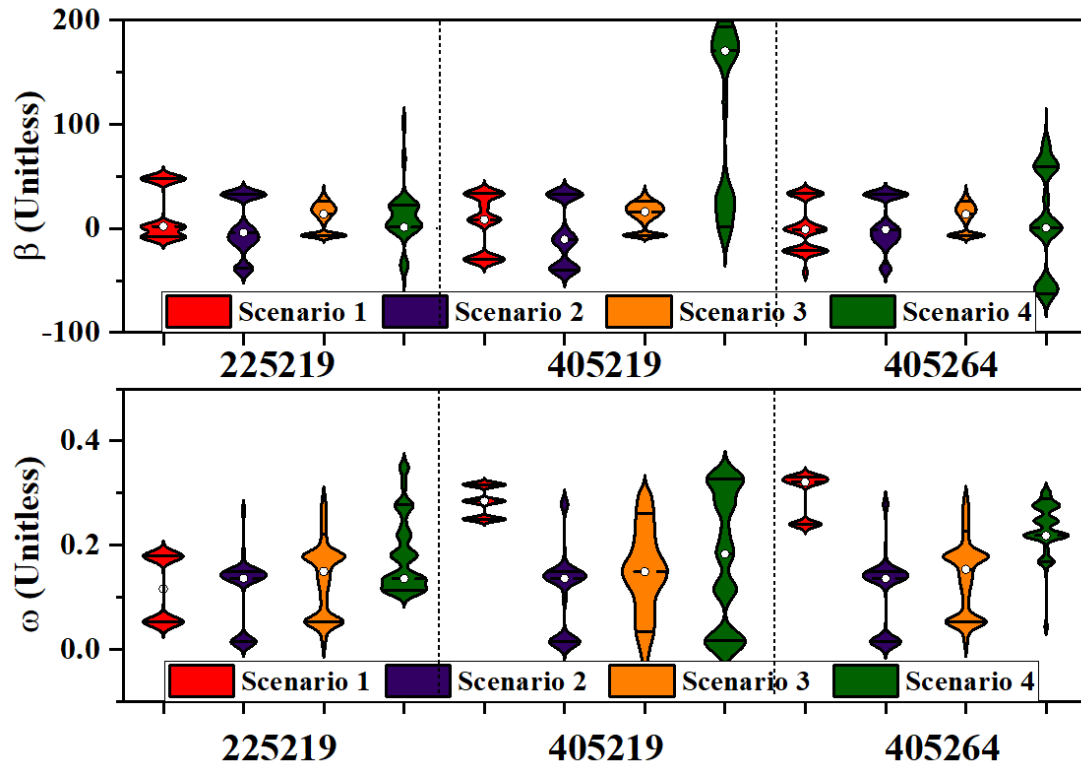


891

892 **Figure 7. Long-term simulation BIAS of  $Q_{\text{median}}$  for five scenarios in all**  
 893 **catchments. Simulation BIAS is plotted as a 10-year moving average, and**  
 894 **10-year moving average streamflows are plotted for reference. The left-hand**  
 895 **three graphs are calibrated in the wet years and then verified in the dry years,**  
 896 **while the opposite sequence applies to the right-hand graphs.**

897

898

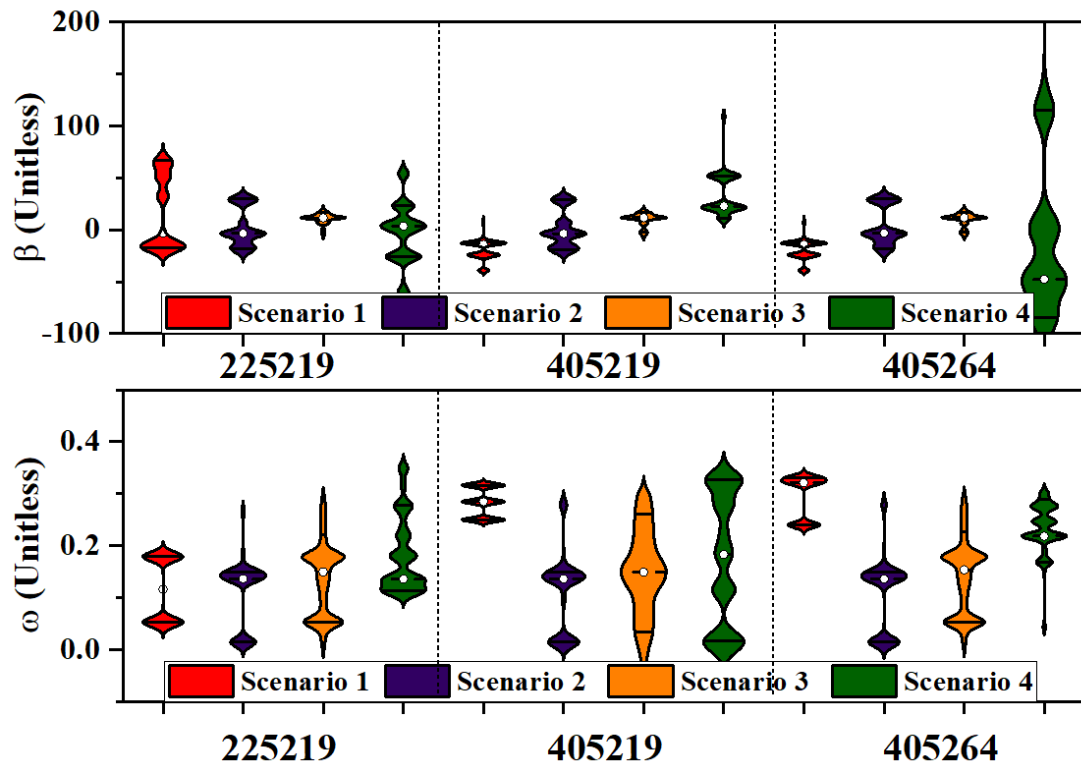


899

900 **Figure 8. Posterior distributions of the regression parameters ( $\beta$  and  $\omega$ ) for the**  
 901 **production storage capacity ( $\theta_1$ ) for the four model scenarios in each catchment**  
 902 **when calibrated in the wet years and verified in the dry years. The solid**  
 903 **horizontal lines within the violin plots denote the 25<sup>th</sup> and 75<sup>th</sup> percentiles of the**  
 904 **posterior distribution, while the white dots denote median estimates.**

905

906



907

908 **Figure 9. Posterior distributions of the regression parameters ( $\beta$  and  $\omega$ ) for the**  
 909 **production storage capacity ( $\theta_1$ ) for the four model scenarios in each catchment**  
 910 **when calibrated in the dry years and verified in the wet years. The solid**  
 911 **horizontal lines within the violin plots denote the 25<sup>th</sup> and 75<sup>th</sup> percentiles of the**  
 912 **posterior distribution, while the white dots denote median estimates.**